Chain Order and Cross-Link Density of Elastomers As Investigated by Proton Multiple-Quantum NMR

Kay Saalwächter*

Institut für Makromolekulare Chemie, Universität Freiburg, Stefan-Meier-Str. 31, D-79104 Freiburg, Germany

Berta Herrero and Miguel Angel López-Manchado

Institute of Polymer Science and Technology (CSIC), C/ Juan de la Cierva 3, E-28006 Madrid, Spain

Received June 13, 2005; Revised Manuscript Received August 19, 2005

ABSTRACT: We present a quantitative study of local segmental order in vulcanized natural and butadiene rubber far above the glass transition. Network chain order is dependent on the density of cross-links and is here derived from proton homonuclear residual dipolar couplings measured by static multiple-quantum NMR spectroscopy at low field. On the basis of a reasonable model of local chain structure and fast, uniaxially symmetric local motions, spin dynamics simulations are used to investigate the relationship between the experimentally determined residual coupling and the order parameter of the polymer backbone. The model is verified by site-resolved determinations of inter- and intraresonance residual couplings at high field. For both types of rubber, it is found that the distributions of the chain order parameter are rather narrow and in all cases well explained by the local coupling topology, thus excluding distributions of end-to-end separations or network chains lengths as important sources of broadening. This suggests that the NMR-detected order phenomenon cannot simply be captured with single-chain concepts. For natural rubber and poly(dimethylsiloxane), the relationship of the cross-link densities derived from the NMR-determined order parameter and from Flory−Rehner swelling experiments is linear as expected, yet the prefactors differ from the prediction by factors of 2 in different directions. We discuss the implications and the validity of the various models and approximations used for data analysis in light of recent results from computer simulations.

I. Introduction

NMR has long been a particularly attractive tool for the study of structure and dynamics of elastomers.[1] Far above the glass transition, results from experiments as simple as Hahn echoes are well-known to be primarily governed by the cross-link density of the investigated rubber. The purpose of the echo experiment is basically to determine the nonrefocusable contribution to the NMR line width in the form of an apparent T_2 or a second moment. The line width is dipolar in origin, resulting from the not fully isotropic motional averaging of couplings within the monomer units subject to restricted fluctuations between cross-links and other topological constraints.[2−4]

While Hahn echoes are still popular, serious criticism has been raised concerning the quantitative analysis of the relaxation curves in terms of residual dipolar couplings and apparent correlation times of slow, cooperative processes.[5−7] Major problems comprise the general validity of the models used for fitting rather featureless intensity decay data, interdependencies among the fitted parameters, and the sensitivity to factors which influence the relaxation behavior but are not covered by the model. Alternatives comprise NMR methods which make a more direct use of the dipolar couplings, such as combinations of Hahn and solid echoes,[2,8,9] two-dimensional (2D) magnetization exchange spectroscopy,[10] and, most recently, double-quantum (DQ) or multiple-quantum (MQ) techniques.[11−17]

The latter class of experiments is particulary powerful in that a very specific intensity buildup related to pairwise couplings is analyzed. Slow-motional effects and pulse sequence imperfections still enter in the form of a damping at longer application times of the pulse sequence, but in more recent work from our own lab it was shown that such effects can be completely suppressed when a proper pulse sequence with a pure DQ average Hamiltonian and a specific normalization protocol is used.[14,16,17] These experiments are further not demanding and can be performed on cost-efficient low-field NMR equipment.[15] We here extend our earlier work on end-linked poly(dimethylsiloxane) (PDMS) model networks to statistically cross-linked rubbers, specifically sulfur-vulcanized poly(*cis*-1,4-butadiene) (BR) and poly(*cis*-1,4-isoprene) (natural rubber, NR).

Although linear relationships between residual coupling-related properties and the cross-link density or the elasticity modulus in such rubbers have frequently been addressed,[10,12,18−25] a unified approach seems to be missing. Exact quantitative relationships are in some cases not discussed and replaced by calibration procedures or are based on ad hoc model assumptions which differ from work to work. Formally, residual interactions are directly proportional to a dynamic order parameter of the polymer backbone,

$$S_b = k\frac{D_{res}}{D_{stat}} = \frac{3}{5}\frac{r^2}{N} \tag{1}$$

and can be calculated from the experimental average residual dipolar coupling constant, D_{res}, by comparison with its static counterpart, D_{stat}. Note that the same

* Corresponding author. E-mail: kays@makro.uni-freiburg.de.

10.1021/ma051238g CCC: $30.25
Published on Web 10/11/2005

argument holds for residual ^{2}H quadrupolar or ^{1}H−^{13}C dipolar couplings. As indicated by the right-hand side of eq 1, S_b is related to r, the ratio of the end-to-end vector to its average, unperturbed melt state ($r^2 = \mathbf{r}^2/\langle\mathbf{r}^2\rangle_0$), and to N, the number of statistical (Kuhn) segments between the constraints.[26] The latter provides the link theories of rubber elasticity, swelling,[27] or stress−optical properties.[28] Below, we present a detailed discussion of the different model assumptions needed for a quantitative assessment of the relationship between S_b and the true cross-link density and highlight the still existing challenges.

Our major focus is the relationship between the NMR observable and S_b, where the constant k in eq 1 comprises details of the local coupling topology and intrasegmental motions. In particular, in earlier works using T_2 relaxometry, D_{stat} was calculated from the static dipolar second moment measured in the glassy state, and k was taken to be unity. This leads to underestimated values for S_b. The Kuhn model requires freely jointed chains, such that a preaveraged uniaxial reference state arising from intrasegmental motions must be defined and subsumed in the constant k.[19] In the spin-pair limit and under the assumption of simple uniaxial rotation of monomer units in fixed conformations, k can be calculated from a Legendre projection of the orientation of the internuclear coupling vector onto the segmental orientation. In addition, the experimental D_{res} is an *apparent* coupling resulting from an average over the complex multispin situation present in real-life monomers, which must also be taken into account for D_{stat} and complicates the picture. In some high-resolution experiments, individual contributions can be unravelled; however, the interpretation often depends on an identification of the dominant couplings in the system, which is often not straightforward, as to be shown herein.

We approach the problem of relating the apparent D_{res} with S_b by using simulations of the NMR response of the local multispin system within the monomers and testing a motional model which is supported by earlier RIS calculations and simulations. For validation, we use site-specific intramonomer couplings which can be resolved using 2D DQ spectra acquired at high field. Our work complements and corrects some of the previous work, in that we show that it is important to consider the full local dipolar coupling topology rather than assuming individual dominant pair couplings and that seemingly reasonable ad hoc assumptions identifying specific C−C bonds with the local backbone direction (which is the symmetry axis of fast motions) may be misleading.

II. Experimental Section

Samples and Characterization. Natural and butadiene rubber were manufactured using standard procedures. NR was kindly supplied by Malaysian Rubber (trade name CV 60), and BR was obtained from Polimeri Europa (trade name Europrene Neocis 40). The latter has about 98% *cis*-1,4-units. The reaction mixtures were prepared in an open two-roll mill, and vulcanization took place at 160 °C in a thermofluid-heated press at the optimum cure time (t_{97}) deduced from the curing curves of a MDR 2000E rheometer. The compositions were 5 phr ZnO, 1 phr each of stearic acid, benzothiazyl disulfide, and phenyl-β-naphthylamine, and different amounts of sulfur in phr indicated by sample name (NR-A0.8, NR-A1, ...). Only one sample of BR was available within the framework of this study (BR-1).

Another series B additionally contained 2.8 phr octadecylamine (ODA) and complemented the NR sample collection toward higher cross-link densities (it is part of a comparative study with organoclay-modified rubber[29,30]). The optimum cure time tends to increase upon increasing the sulfur amount, but sensibly decreases by adding ODA. This acceleration of the vulcanization reaction is well-known and has also been observed for other primary and secondary amines (see refs 30 and 31 and references therein). The average mass of network chains M_c was determined on the basis of equilibrium swelling experiments (taking about 72 h) using toluene at 30 °C by application of the modified Flory−Rehner equation[32],

$$-\ln(1-\phi_r) - \phi_r - \chi\phi_r^2 = \frac{\rho V_0}{M_c}[\phi_r^{1/3} - {}^1/_2\phi_r] \qquad (2)$$

where ϕ_r is the polymer volume fraction in the swollen network (the reciprocal swelling degree Q), V_0 is the molar volume of the solvent (106.2 mL/mol for toluene), ρ is the density of the rubber (0.92 g/cm^3 for NR), and χ is the Flory−Huggins polymer−solvent interaction term (0.393 for NR/toluene). Note that M_c is obtained as a number average. Equation 2 is valid for 4-functional cross-links, and in this case, the number of cross-links equals the number of elastically active chains per unit volume and is given by $\bar{n} = \rho/M_c$.[27]

NMR Spectroscopy. ^{1}H MQ experiments were performed following previously published procedures.[14,16,17] A pulse sequence of variable duration τ_{DQ} featuring a pure DQ average Hamiltonian was used,[33] which is able to excite all even quantum orders in a multispin system. The same pulse sequence block is applied to reconvert the higher-order MQ coherences into observable magnetization, and a phase cycling scheme is used to select a DQ-filtered (I_{DQ}) and a reference (I_{ref}) intensity. I_{DQ} subsumes signal from dipolar coupled segments and all $4n + 2$ quantum orders (as a result of the four-step selection phase cycle). I_{ref} contains contributions from all $4n$ quantum orders as well as dipolar-encoded longitudinal magnetization plus all signal from uncoupled, i.e., isotropically mobile components. The sum $I_{DQ} + I_{ref}$ comprises the full magnetization of the sample subject to relaxation and is used to *normalize* the DQ-filtered intensity, thereby removing any influence of slow motions and other relaxation effects on the data. Before doing so, the uncoupled contributions (sol, dangling ends), which appear as very slowly relaxing tails of I_{ref}, are quantitatively determined and subtracted. See ref 17 for details on this procedure. The normalized DQ buildup data, subject to further analysis, is hence obtained as

$$I_{nDQ} = \frac{I_{DQ}}{I_{DQ} + I_{ref} - B\exp\{-2\tau_{DQ}/T_{2B}\}} \qquad (3)$$

$I_{ref}(\tau_{DQ}=0)$ corresponds to the full magnetization of the sample measured after a 90° pulse, and when the data are represented relative to this intensity defining unity, B is the proton integral fraction of the mobile components.

From about 50 K above the glass transition, the normalized DQ buildup data are temperature-independent over many tens of Kelvin, providing evidence that slow-motional effects are largely absent in I_{nDQ}. Using only intensities $I_{nDQ} \leq 0.45$, the normalized DQ buildup curves are analyzed with a buildup function based on a static second-moment approximation[14,16,17]

$$I_{nDQ}(D_{res}) = \frac{1}{2}\left(1 - \exp\left\{-\frac{2}{5}D_{res}^2\tau_{DQ}^2\right\}\right) \qquad (4)$$

Note that D_{res} is an *apparent* coupling constant and represents an average over many different internuclear pair couplings. Marked deviations of the buildup data from an inverted

Gaussian indicate the presence of a substantial distribution. Assuming this distribution to be Gaussian,[14] the relation

$$I_{\mathrm{nDQ}}(D_{\mathrm{G}},\sigma_{\mathrm{G}}) = \frac{1}{2}\left(1 - \frac{\exp\left\{-\frac{\frac{2}{5}D_{\mathrm{G}}^2\tau_{\mathrm{DQ}}^2}{1+\frac{4}{5}\sigma_{\mathrm{G}}^2\tau_{\mathrm{DQ}}^2}\right\}}{\sqrt{1+\frac{4}{5}\sigma_{\mathrm{G}}^2\tau_{\mathrm{DQ}}^2}}\right) \qquad (5)$$

can be used to determine an average coupling constant as well as estimate the standard deviation (D_{G} and σ_{G}, respectively). Note that fits to this function make physical sense only as long as σ_{G} is substantially smaller than D_{G}. Numerical inversion procedures can otherwise be used to assess the distribution.[14]

The complete series of rubbers was investigated on a Bruker minispec mq20 operating at 0.5 T (90° pulses of 1.9 μs length), which we have previously shown to produce fully quantitative results.[15] Site-resolved experiments for the derivation of the model for data analysis were further conducted on a Bruker Avance 500 solid-state NMR spectrometer ($B_0 = 11.7$ T) using the proton channel of a commercial static double-resonance probe (3 μs 90° pulses). The experimental protocol is flexible in that $\tau_{\mathrm{DQ}} = n_{\mathrm{c}}t_{\mathrm{c}}$ can be incremented by either using a fixed number of pulse sequence cycles n_{c} and varying the cycle time t_{c}, or vice versa. On the minispec, the time-incremented two-cycle version ($n_{\mathrm{c}} = 2$) is the more robust choice, while at high field, the n_{c}-incremented version with cycle times of $t_{\mathrm{c}} = 200$ and 800 μs is used. This provides rapid refocusing of shift and susceptibility effects and therefore suppresses dipolar second-averaging effects[7] and the influence of isotropic J couplings. Note that τ_{DQ} is always corrected by a duty-cycle-dependent scaling factor $a(\psi)$.[14]

All NMR experiments were performed at sample temperatures of 80 °C. Sulfur-vulcanized rubbers tend to age, and extended experimentation at this temperature over many days leads to a notable increase of the order parameter. Storage at room temperature leads to increases on the 10% level over a time scale of weeks. Thus, NMR and swelling experiments were performed in close timely coincidence.

Spin Dynamics Simulations. The MQ-NMR response of protons in the monomer units of NR and BR was calculated with a home-written matrix-based spin-dynamics code which is in many respects similar to the publicly available SIMPSON software.[34] It is based on a stepwise integration of the Liouville−von Neumann equation, employs a product-space representation of the spin operators and the density matrix, and uses series expansions for the calculation of the propagators. The pulse sequence is calculated explicitly as a succession of pulses and free-evolution intervals. Selection of higher-quantum coherences after the excitation period is performed by retaining the appropriate entries in the density matrix and nulling all others, which is more efficient than (yet equivalent to) the explicit calculation of a phase cycle.

The spin system parameters are entered in terms of Cartesian coordinates of the individual spins, from which the dipolar coupling tensors are calculated. We have used common values for the different bond lengths and angles. Therefore, the couplings, order parameters, and cross-link densities derived on the basis of the model calculations may be underestimated by 20% due to the neglect of fast vibrational averaging. We did not attempt to take these into account, as such effects are presumably different for inter- and intragroup couplings, which are of similar magnitude in our model.

The software permits the calculation of averages of interaction tensors associated with specific spins. This feature was for instance used to mimic the effect of conformational jumps of CH_2 groups by taking an average over the tensors associated with a specific out-of-group proton and the two methylene protons. The effect of the C_3 rotation of methyl groups in NR on the intra- and intergroup couplings was considered in the same way. In addition, uniaxial rotation of the monomer unit around the z-axis, with arbitrary relative orientations of the arrangement of spins specified by Euler angles, is also realized by calculating averages of all interaction tensors in the spin system over three symmetrically arranged positions around the rotation axis. Owing to the rotational symmetry of the dynamically averaged spin system, a minimum of 20 crystallite orientations with Euler angles β (rotation around the y-axis) equally spaced from 0° to 90° was sufficient to reach convergence of the powder average at least for the τ_{DQ} intervals shown in the figures. Convergence was checked by testing considerably higher numbers of orientations.

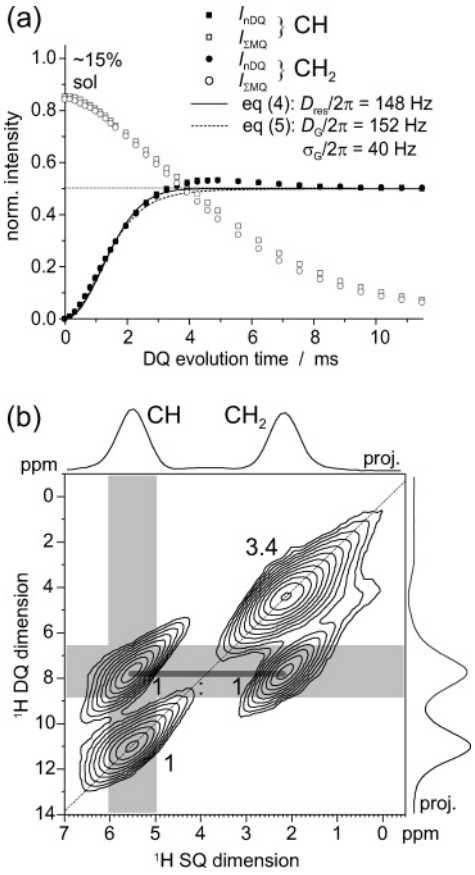

Figure 1. Site-resolved DQ buildup data (a) and 2D DQ correlation spectrum of BR-1 with $\tau_{\mathrm{DQ}} = a(\psi) \times 8 \times 200$ μs = 1.312 ms (b) acquired at high field. The projections in (b) are summed over the gray shaded areas, and the numbers represent the relative peak areas.

III. Results and Discussion

In the following, we first present the NMR spectroscopic findings which are relevant for the evalutation of motional models for *cis*-diene rubbers, then turn to model calculations of the local spin system response of fluctuating polymer segments and the resulting determination of a backbone order parameter, discuss the distribution of residual couplings experimentally found in NR, and finally address the relationship between the experimentally determined order parameter and the actual cross-link density. This section also includes a comparison with the independent macroscopic characterization of the sample series by equilibrium swelling measurements. To conclude, we discuss the significance of the results in relation to previous work.

A. Site-Specific Segmental Mobility. The high-field DQ buildup curves shown in Figure 1a represent a first insight into the dynamics of CH and CH_2 groups in BR. Their behaviors, and thus the average residual couplings to their next neighbors, appear almost identical. While different rise times, and thus different residual couplings, would not be unexpected, the iden-

tity of the long-time behavior, i.e., the approach of a plateau at 50% of the full initial magnetization, is a necessary observation, as MQ coherences will always spread equally over the full spin system, with a 1:1 partition into $4n + 2$ and $4n$ coherence orders.[14] The 2D DQ spectrum in (b) aids to unravel the contributions of couplings of the detected spin to like and unlike spins, represented by the spectral intensities associated with the autopeak located on the DQ diagonal and the cross-peak connecting the two signals in the SQ dimension at the same vertical position in the DQ dimension, respectively.

A series of such 2D spectra may be used to construct corresponding individual buildup curves, as was demonstrated in an important paper by Spiess and coworkers.[11] Their analysis is, however, subject to some restrictions to be highlighted in the next section. Specifically, such buildup curves are constructed on an intensity scale set by the contributions of the individual DQ intensities relative to the total magnetization. The interpretation of these curves in terms of orientation-specific order paramters is crucially dependent on assumptions concerning the local coupling topology, i.e., the number of individual pair couplings. In the cited work, only single dominant pair couplings were assumed, and the couplings were mapped onto results from RIS simulations to interpret the different order paramters. Earlier work on site-resolved couplings[10] was based on the more restrictive interpretation in terms Legendre projections of the associated dipolar tensor orientations onto an assumed symmetry axis of motion. It will be shown below that such model assumptions are critical.

Nevertheless, the site-specific buildup behavior of a specific functional group and the partition of its DQ intensity into interactions with its chemically different neighbors contains valuable information on the segmental dynamics. In the following, we focus the discussion on the ratio of the average residual couplings detected at the different sites (1:1 in the present case) and on the cross contributions from the different resolved coupling partners to the respective full DQ intensities taken from 2D spectra (0.5 for the CH group and $1/(1 + 3.4) = 0.23$ for the CH_2 group).

These observations were a strong function neither of the actual DQ evolution time nor of the cross-link density, as checked on different samples of our NR series. Corresponding data for NR were published previously under different cover,[7] and the major observations were (i) also an approximate 1:1 ratio for average couplings detected at the CH and $CH_{2,3}$ positions (the methyl and methylene resonances are not resolved in static spectra) and (ii) an average 12% cross-signal fraction detected at the $CH_{2,3}$ resonance. The cross-signal fraction detected for CH is 86% because the moiety is isolated, and since the modeling of the long =CH···HC= distance would necessitate the treatment of all in-between spins, we chose to not consider this constraint for reasons of computation effort.

B. Model for Local Dynamics. As mentioned, previous studies[10,11] have identified specific backbone bonds with the preferred ordering axes for segmental motions, and specifically, Legendre projections of (allegedly) proton pair-specific order parameters onto such a direction were used to derive an order parameter for the backbone.[10] The intricacies of such approaches were thoroughly discussed in an earlier paper by Fry and Lind for the example of a polyethylene chain.[19] In the first publication on site-resolved DQ measurements, the C=C double bond was identified with the direction of highest order for poly(1,4-butadienes).[11,35] This scenario is put to a test below. Before, we point out the arguments that back up the choice of an improved model.

First, uniaxial symmetry is assumed. This is common practice and has the advantageous consequence that any process beyond simple rotation around this axis is subsumed in an overall scaling of all couplings in the system by S_b. While using rotational averaging of a fixed molecular segment around a chosen axis is certainly a convenient choice, it does not take into account conformational jumps, which are after all the true basic processes in chain motion. Averaging over the H···H distances involved in jumps around a specific C−C bond is possible when this bond is taken as the symmetry axis of motion,[10] but a more general procedure is necessary when an extended spin system is to be simulated.

We chose to use the *crystal structures* of BR[36] and NR[37,38] as reference chain structures, which is motivated by the notion that the chain conformation in the crystal is usually close to the lowest-energy state. Conveniently, BR and NR share the same backbone conformations (*s_+-cis-s_+-t-s_--cis-s_--t-*), such that one of the CH protons of BR can just be replaced by a methyl group to obtain the NR structure. The BR structure is shown in Figure 2. RIS calculations[39] and related approaches[40] as well as atomistic Monte Carlo simulations of the melt state[41] agree in that the most populated state of the CH_2-CH_2 bond is indeed *trans*, while the CH_2-CH bond is dominated by *skew* conformations.

Conformational jumps between *skew*$_+$ and *skew*$_-$ (as well as the methyl rotation in the case of NR) are mimicked by calculating averages of the involved coupling tensors. Thus, the two protons of a given methylene group are always equivalent in their couplings to the surroundings, notwithstanding the underlying static chain structure. Fast rotational averaging around an assumed local backbone direction is performed, and importantly, different orientations are tested. Figure 2 defines the Euler angles β and γ used to locate this axis within the chain segment. The basic assumption of our approach is that these averaging steps are adequate to parametrize the segmental dynamics within a single freely orientable (Kuhn) chain segment.

The spin dynamics simulations were performed with a varying number of protons in order to test the importance of couplings to the different nearby protons. Final DQ intensities are always evaluated for one proton of a given type (the "reporter spin," printed in bold in Figures 2−5) and plotted relative to its initial polarization taken to be unity. Simulations with more than eight spins are not feasible due to the excessive size of the corresponding density matrix. By varying the participating spins in simulations with fewer spins, it was always possible to identify the nuclei which are most strongly coupled to the respective reporter spin, and these were used in the final eight-spin calculations.

The integral DQ buildup curve, accessible in low-field experiments, is then constructed as a weighted average and fitted to eqs 4 and 5 to obtain a reference coupling and estimate the width of its apparent distribution. Note that there are two different types of CH_2 groups in NR and a lifted degeneracy once the rotation axis is tilted away from the double bond direction. The shown data

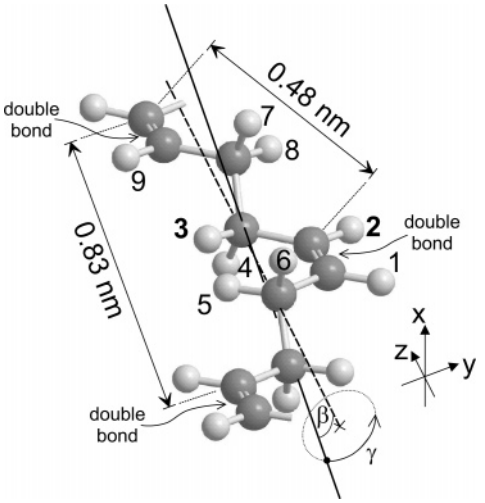

Figure 2. Model of the chain structure of *cis*-BR adopted from the crystal structure. For NR, protons 1, 2, or 9 can be replaced by a CH_3 group. The dashed line points along the z-axis, which also coincides with the C=C double bond, and the Euler angles β and γ (pseudo-active rotations around y and z, respectively) define the symmetry axis of motion used in the simulations. The crystalline backbone is oriented at $\beta = 17.7°$, $\gamma = 0$.

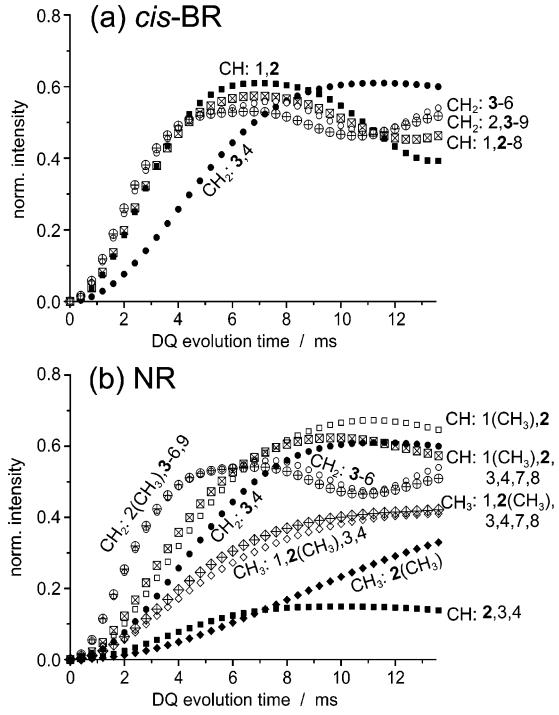

Figure 3. Simulated DQ buildup curves for BR (a) and NR (b) for segmental rotations around the double bond direction ($\beta = 0$, $\gamma = 0$). The numbers refer to the accounted protons with positions specified in Figure 2; the nomenclature is further explained in the text.

are always averaged over the corresponding individual buildup curves. All simulated curves are calculated using a scaling factor of 0.01. This corresponds to a backbone order parameter of the same magnitude and should facilitate a comparison of the graphs to experimental data, where the buildup occurs on a similar time scale. Note that this scaling factor is arbitrary, as it applies to all couplings due to cylindrical symmetry. The static-limit reference coupling is thus obtained from the fitted couplings as $D_{stat}/k = 100D_{res}$.

Figure 3 shows results for buildup curves calculated for the CH, CH_2, and CH_3 resonances of BR and NR for the case where the dynamics is taken to be uniaxially symmetric around the double bond direction. The no-

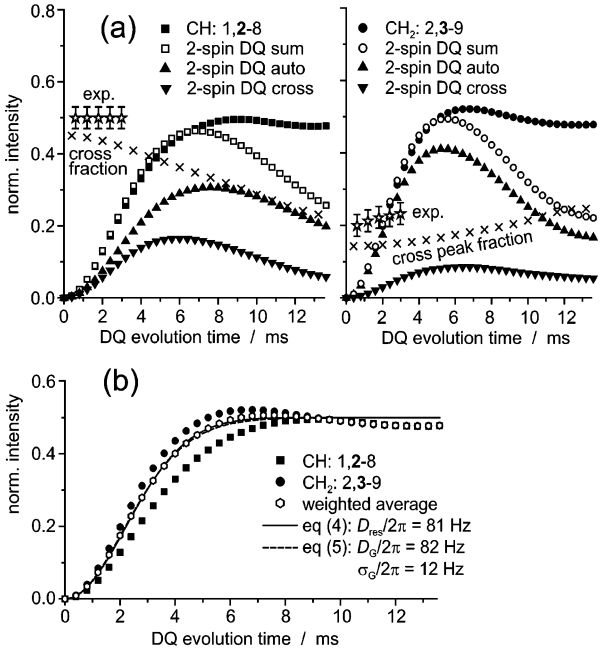

Figure 4. Simulated DQ buildup curves for BR for segmental motions around an axis oriented at $\beta = 30°$, $\gamma = 0$. In (a), the partition of the buildup behavior of the individual groups into two-spin DQ auto- and cross-contributions is shown and compared with experimental cross-peak fractions from 2D DQ spectra, for which the time axis was scaled appropriately. In (b), the site-specific buildup curves are compared with their weighted average and the fitting results.

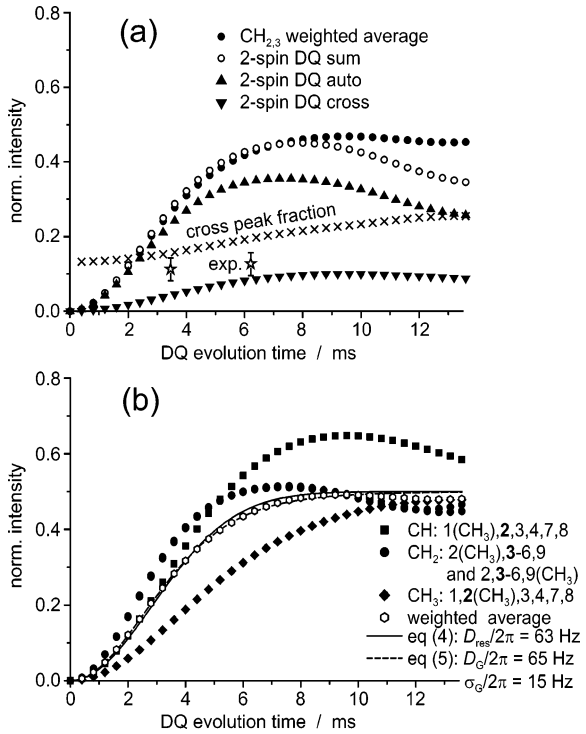

Figure 5. Simulated DQ buildup curves for NR for segmental motions around an axis oriented at $\beta = 20°$, $\gamma = 0$. In (a), the partition of the average CH_2 and CH_3 buildup into two-spin DQ auto- and cross-contributions to the CH proton is shown and compared with experimental cross-peak fractions from 2D DQ spectra, for which the time axis was scaled appropriately. In (b), the site-specific buildup curves are compared with their weighted average and the fitting results.

menclature is as follows: The "reporter spin" representative for each of the groups (CH, CH_2, and CH_3) is printed in bold. All spins used in the respective simulations are enumerated, where e.g. 1,**2**-8 means that spin 2 is detected and all spins between number 1 and 8 as defined in Figure 2 participate. **2**(CH_3) means that proton number 2 is replaced by a methyl group, which is also detected.

For both BR and NR, the buildup associated with the CH_2 groups (circles) clearly demonstrates the shortcomings of interpreting such data in terms of individual local couplings: variation of the secondary spins shows that the strongest coupling is not the intra-CH_2 coupling, but the interaction with the other spectroscopically indistinguishable CH_2 group across the double bond. This is not surprising, as the *skew* conformations lead to rather close interproton distances, with average internuclear vectors which are along the double bond and thus not averaged considerably by rotation (as opposed to the intra-CH_2 coupling). A similarly strong dependence on different remote spins is also observed for the methyl group of NR. In that case, the methyl group is also identified as the most important passive coupling partner for the CH proton.

In all cases, it is seen that the inclusion of more spins beyond the dominant ones change the initial buildup only weakly, while the behavior toward the maxima and into the plateau regions of the curves still changes appreciably and cannot be taken as representative of experimental data. The ultimate smearing-out of the oscillations around $I_{nDQ} = 0.5$ to form a well-discernible plateau and the observation of identical behavior for the different functional groups in this region is not attainable with eight-spin simulations. Yet, fits to the initial behavior for $I_{nDQ} \leq 0.45$ are expected to yield representative results.

The eight-spin simulation data in Figure 3a are in principle compatible with the experimental observation that the buildup behaviors detected at the aliphatic and olefinic resonances are similar in BR (see Figure 1a). However, when calculating the partition of the DQ intensities into auto- and cross-contributions, we found that the cross-contribution for the CH group does not exceed 10%, with 50% being the experimental finding (see Figure 1b). For NR, the scenario is also not able to satisfactorily account for the experimental data. Therefore, the assumption that the local motions can be analyzed on the basis of rotational symmetry around the double-bond direction does not hold.

To obtain more reliable values for the integral static limit reference couplings, a large number of buildup curve simulations were performed, in which the orientation of the symmetry axis for rotational averaging was changed. The angles β and γ defined in Figure 2 were varied between 0° and 40° in steps of 10° and between 0° and 90° in steps of 30°, respectively, thus sweeping a reasonable range of average segmental orientations with some degree of correlation to the C−C directions in the reference chain structure. Such a tilt could model the effect of subsequent or correlated conformational jumps, resulting in crankshaft-type reorientations of individual bonds. However, one should not overrate the significance of these angles; they mainly serve to parametrize a more complex behavior and provide an idea about the symmetry. The results were checked against the experimental constraints, which are the 1:1 ratios of the apparent couplings detected at the aliphatic and olefinic resonances, and the observed partition of DQ intensities taken from the 2D spectra.

It turned out that the given constraints are rather strong in that they could not be matched perfectly for the same set of angles, indicating the limits of the model. We here just discuss the data sets corresponding to the "best fits". The data in Figures 4 and 5 show that best agreement could be attained with β between 20° (NR) and 30° (BR), and $\gamma = 0$ in both cases. Note that the polymer backbone in the crystal structures is oriented at $\beta = 17.7°$, $\gamma = 0$. All other sets of trial angles lead to more serious discrepancies for at least one of the experimental constraints.

The static limit reference couplings, obtained by fitting the averaged buildup curves in Figures 4b and 5b for $I_{nDQ} \leq 0.45$, are

$$\text{BR: } D_{stat}/k = 2\pi \times 8.1 \text{ kHz} \quad (6)$$

$$\text{NR: } D_{stat}/k = 2\pi \times 6.3 \text{ kHz} \quad (7)$$

These values can be used to calculate backbone order parameters S_b according to eq 1. The apparent distribution of residual couplings, which parametrizes intrinsic deviations from an inverted-Gaussian shape and the underlying distributions of pair couplings, is rather narrow. The standard deviation is less than 25% of the average coupling in both cases and somewhat broader for NR due to the more weakly coupled contribution from the methyl group. Therefore, an experimental observation of a wider distribution would certainly be indicative of semilocal network heterogeneity.

One final comment should be added on the procedure used for calculating the DQ intensity partitions and its implications. In Figures 4a and 5a, the solid squares and circles denote the integral olefinic and aliphatic DQ intensities, respectively, where DQ-filtering in the density matrix was in accordance with the experimental four-step DQ filter, which keeps all $2n + 2$ coherence orders, including mixed multispin DQ coherences of the type $(\hat{I}^i_+ \hat{I}^j_+ \pm \hat{I}^i_- \hat{I}^j_-)\hat{I}^k_+ \hat{I}^l_-$, which result from several consecutive DQ transitions involving different pairs. When *pure two-spin* DQ coherences ($\hat{I}^i_+ \hat{I}^j_+ \pm \hat{I}^i_- \hat{I}^j_-$) are selected (open symbols), marked deviations occur in the region around and beyond the first maxima. Earlier spin counting experiments have shown that higher-order (4Q, 6Q, etc.) coherences do not contribute appreciably before well into the plateau region,[14] and the mixed multispin coherences are thus identified as most important contributors to the intermediate-time response in multispin systems. Again, the deviations are minor in the significant rising parts, where it can also be seen that the earliest of these mixed coherences even lead to a very weak damping of the integral DQ intensity. The partitions, to be compared with the 2D spectra, were selected on the basis of two-spin DQ coherences involving spins of same (auto) or different (cross) type as the reporter spin.

In summary, the results of this section indicate that a reduction of the analysis of site-resolved residual couplings to dominant pair couplings may lead to incorrect conclusions on the symmetry of local chain motions and systematic errors for the chain order parameters calculated from eq 1. Improvements over our still crude model would certainly be possible by explicitly using dipolar couplings averaged through a computer simulation run. Additional experimental con-

Table 1. Results of the MQ NMR and Swelling Analyses of NR and BR[a]

	MQ NMR							swelling	
sample	B (%)	$D_{res}/2\pi$ (Hz)	S_b	M_c (g/mol)	$D_G/2\pi$ (Hz)	$\sigma_G/2\pi$ (Hz)	σ_G/D_g	ϕ_r	M_c (g/mol)
NR-A0.4	11.6	100	0.016	6170	103	26	0.25	0.076	38957
NR-A0.8	9.4	129	0.021	4775	132	27	0.20	0.108	21175
NR-A1	14.4	134	0.021	4612	138	34	0.25	0.111	20771
NR-A2	6.3	170	0.027	3630	174	36	0.21	0.150	11244
NR-A2.5	4.2	208	0.033	2966	208	33	0.16	0.173	8867
NR-A3	4.6	197	0.031	3136	200	44	0.22	0.171	8285
NR-A4	3.8	218	0.035	2824	221	50	0.23	0.182	7149
NR-A6	2.8	252	0.040	2452	255	49	0.19	0.193	6823
NR-A10	2.7	295	0.047	2090	298	66	0.22	0.215	5256
NR-B1	4.6	196	0.031	3148	196	30	0.15	0.160	10559
NR-B2	2.6	280	0.045	2200	279	45	0.16	0.198	6506
NR-B2.5	2.8	314	0.050	1965	314	33	0.11	0.216	5362
NR-B3	4.1	321	0.051	1924	317	88	0.28	0.219	5152
NR-B4	1.9	365	0.058	1689	369	54	0.15	0.235	4354
BR-1	15.0	148	0.023	5360	152	40	0.26		
PDMS47200	0.3	185	0.024	6843	183	51	0.28	0.192	10759
PDMS5200	2.9	357	0.047	3546	377	111	0.29	0.323	2684
PDMS780	0.1	987	0.130	1283	1109	493	0.44	0.526	584

[a] The data are compared with previous data for end-linked PDMS networks,[14,43] where the sample name indicates the number-average precursor molecular weight M_{pre}. For the swelling analysis of PDMS networks using eq 2, $\rho = 0.97$ g/cm^3 and $\chi = 0.45$.[44]

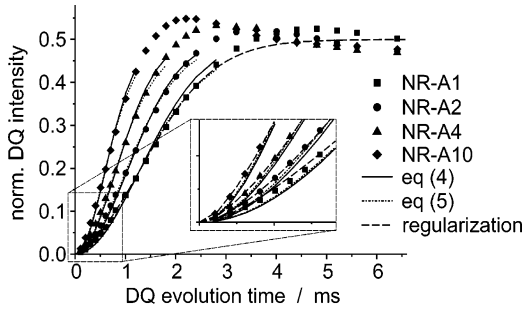

Figure 6. DQ buildup data for different samples of NR measured at low field. The curves indicate rather narrow distributions of residual couplings, but feature a weak second contribution with stronger couplings, which can only be captured by numerical inversion (see inset).

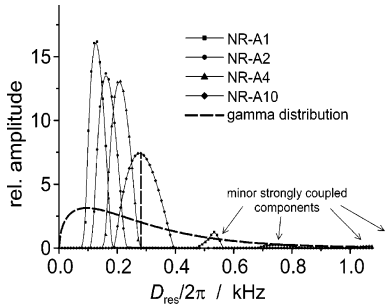

Figure 7. Distribution functions of residual couplings for the sample data shown in Figure 6, obtained by regularization analysis.[14] The gamma distribution results from a Gaussian distribution of end-to-end separations; its average is scaled to the average for NR-A10.

straints might also be taken from magic-angle spinning (MAS) or heteronuclear dipolar experiments,[11,42] where increased site resolution can be taken advantage of and more details of the models can be tested. However, preliminary $^{13}C-^{1}H$ experiments from our lab (both static and under MAS) indicated that also in this case a restriction to intragroup couplings and simplified data analyses in terms of fixed bond orientations and Legendre projections is not straightforwardly possible.

On the positive side, the body of our many simulations suggests that the results for the reference couplings D_{stat}/k and thus the backbone order parameters are not very sensitive to the model and should be precise within 20%. For example, for the various motional symmetry axis orientations in BR, the strongest observed coupling was 10.5 kHz and the weakest 6.4 kHz, with the average at 8.4 ± 1.2 kHz, which is close to be "best-fit" value of 8.1 kHz.

C. Residual Couplings and Their Distribution in NR. The model for the quantitative determination of the backbone order parameters is now tested on a series of NR at different levels of cross-linking. Representative buildup curves are plotted in Figure 6, and the results from the fits to eqs 4 and 5 are collected in Table 1. From Figure 6, it is apparent that the distributions of the residual couplings are rather narrow, as the two fits are rather similar. In fact, the ratios σ_G/D_G reported in Table 1 are not significantly larger than what is expected from the local coupling topology assessed in our simulations. Therefore, any other type of distribution, as to be expected from the Gaussian distribution of end-to-end separations and the polydispersity of the network chains, does not exert appreciable influence on the NMR observable.

The actual distributions obtained by regularization analysis of the buildup curves plotted in Figure 7 provide a convincing visualization. In all networks, a small minority component (~10%) with significantly enhanced coupling is identified. Because of its large separation, it is not captured by the fitting functions, and the D_G and σ_G from eq 5 agree very well with the regularization result for the dominant fractions. This also provides a consistency check of the numerical procedure. The highly ordered part probably arises from heterogeneities in the network structure, whose origin will have to be clarified in more systematic studies.

The distribution for NR-A10 is compared with a gamma distribution of the same average, which is expected for a Gaussian distribution of end-to-end separations.[14,45] The difference is dramatic, and the phenomenon was also found in Monte Carlo simulations of the NMR response of end-linked networks.[43,45] Our current interpretation is that at short end-to-end separations the chain does not probe the theoretically required conformational space due to its increased probability of being involved in topological constraints ("trapped entanglements"). Thus, the order of these chains is higher than expected. These arguments do not

yet take into account the distribution of network chain lengths, which is exponential in statistically cross-linked long-chain systems.[27,46] This further aggravates the significance of the observed narrow distribution and suggests that the chain order phenomenon detected by NMR is not simply related to the length of a single network chain. This represents a serious *caveat* for the validity of eq 1, and some insight into the real picture can be taken from simulations of monomodal end-linked networks.[43,45]

These findings are in substantial disagreement with earlier experiments using ^{2}H NMR,[47] where so-called "super-Lorentzian" line shapes were observed and theoretically related to Gaussian chain statistics.[48,49] We believe that such observations can arise from slow dynamic processes, and sol and dangling chains contributing a sharp spectral center. These effects cannot easily be separated with 1D spectra alone. Support of our statement is provided by data of Kornfield et al.[50] and our own natural-abundance ^{2}H spectra on PDMS networks with very low sol and dangling-chain contents. These exhibit shapes which are much closer to Gaussians (data to be published).

D. Relationship to Network Structure. To obtain information on the actual chemical structure of a network by use of eq 1, one has to relate the number of Kuhn segments N of the equivalent chain to the actual number of monomer units. Note that the prefactor $^3/_5$ in eq 1 results from the assumption of Gaussian statistics for the end-to-end vector $\mathbf{r}$.[26] The desired relation can be derived from the usual models for semiflexible chains. Chain stiffness is most commonly parametrized by Flory's characteristic ratio[51]

$$C_\infty = \frac{\langle \mathbf{r}^2 \rangle_0}{4nl^2} = \frac{N{l_K}^2}{4nl^2} \tag{8}$$

Here, n is the number of monomer units, $4n$ the number of backbone bonds for the case of poly(1,4-diolefins), and l their root-mean-square bond length $[(1.34^2 + 1.54^2 + 2 \times 1.51^2)/4]^{1/2} = 1.48$ Å). The Kuhn segment length l_K and the contour length L are related to the molecular dimensions via $L = Nl_K = c4nl$. Using this relation to eliminate l_K from eq 8, the molar mass between cross-links is calculated as

$$M_c = nM_0 = \frac{NC_\infty}{4c^2} M_0 \tag{9}$$

with M_0 as the molar mass of the monomer unit (68.1 g/mol for NR). For BR and NR, simulations and experimental work agree on average values of $C_\infty = 4.9$ and 4.7, respectively.[39,41,52]

Note that L arises in a straightforward manner for the extended freely jointed Kuhn chain, yet a certain arbitrariness is expressed in the factor $c = l_p/l$, which depends on the projection length l_p of the bond onto the backbone at its maximum extension, as a result of valence angle restrictions (see Appendix G of ref 51). The projection length is not a unique quantity in polymers with different types of backbone bonds, and we here propose to refer to the crystal structure (Figure 2) and use $c = 0.83$ nm/$(8 \times 0.148$ nm$) = 0.7$. While a somewhat more extended structure is still possible, it

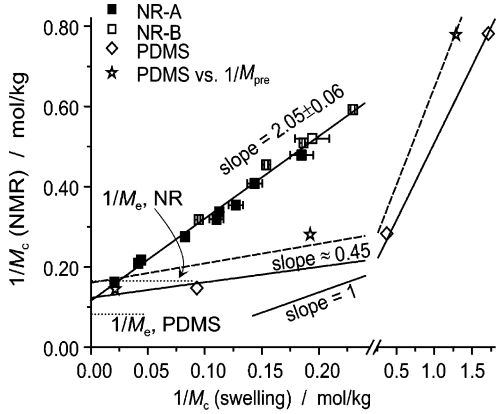

Figure 8. Comparison of NMR-determined reciprocal inter-cross-link molecular weights of NR with corresponding results from swelling experiments. The data are contrasted with our previous results for PDMS.[14,43]

is energetically disfavored. Using $c = 0.7$ in eq 9 and combining with eqs 1 and 7 leads to

$$M_c^{(NR)} = \frac{3 \times 6300 \text{ Hz}}{5D_{res}/2\pi} \frac{4.7}{4 \times 0.7^2} M_0 = \frac{617 \text{ Hz}}{D_{res}/2\pi} \text{ kg/mol} \tag{10}$$

for the inter-cross-link molecular weight of natural rubber.

The significance of c has been the subject of some confusion in the literature, as $c = 1$ leads to the incorrect statement that C_∞ is the number of backbone bonds per Kuhn segment. This assumption is used in several NMR papers, including our own ones on PDMS.[14,43] The resulting deviation is not too large for polymers with large valence angles but must be taken into account for polyolefins.

Here, it should be mentioned that Flory's approach to use the extended polymer chain as a reference state has recently been criticized, as it implies that the chain *inside* a Kuhn segment is also fully extended, which need not be the case.[53] These arguments were brought forth because the onset of Rouse-type dynamic behavior and the possibility to describe chains as Gaussian was observed to set in at much different chains lengths in polymers with similar values for C_∞. Therefore, future work along these lines will have to show to which extent the whole model framework underlying the derivation of eqs 1 and 9 can hold. As also shown recently,[28] RIS-based simulations might provide a viable means to achieve a better understanding.

In Table 1 and Figure 8, we compare the present data with our results for end-linked PDMS model networks.[14,43] In these publications, the fits were performed with a specific buildup function taking into account the particularities of MQ excitation in methyl groups. It differs from eq 4, which is based on a second-moment approximation for spin pairs, by a prefactor of 2.02. For continuity, we here suggest to analyze data from PDMS networks also with eq 4 or 5, resulting in apparent pair couplings which are a factor of 1.4 larger. The correct static-limit reference coupling, derived from the model simulations in ref 14, is then

$$\text{PDMS: } D_{stat}/k = 2\pi \times 7.58 \text{ kHz} \tag{11}$$

Order parameters calculated with this value are then about 20% lower than the previously reported ones, as the previous reference coupling was an experimental

value for rigid methyl groups, which is partially preaveraged by fast bond vibrations, which are ignored here. The resulting relation for M_c reads

$$M_c^{(PDMS)} = \frac{3 \times 7580\ \text{Hz}}{5D_{res}/2\pi} \frac{5.8}{2\left(\frac{0.29}{2 \times 0.165}\right)^2} M_0 = \frac{1266\ \text{Hz}}{D_{res}/2\pi}\ \text{kg/mol} \quad (12)$$

where we have now fixed our previously incorrect use of C_∞. The correction amounts to a factor of 1.3, which does not affect the qualitative conclusions of refs 14 and 43.

The NMR-determined network parameters can now be compared with results from the swelling experiments. In the following, we implicitly assume that swelling gives correct data for the (chemical plus physical) cross-link densities. A detailed criticism of this assumption is beyond the present scope, but support is given by the consistent results for end-linked PDMS, where the precursor molecular weight M_{pre} is known. In Figure 8, $1/M_c$ determined by NMR is plotted vs $1/M_c$ from swelling. In this representation, the data are proportional to the cross-link density ($\bar{n} = \rho/M_c$), and the NMR values scale linearly with both D_{res} and S_b. Convincing linear relationships are found. The linearity of NMR observables and macroscopic network parameters has been reported frequently using a variety of NMR experiments,[10,12,19,21,22] and our above model considerations allow us to discuss this proportionality now in a more quantitative fashion.

Note that NMR methods which rely on the evaluation of the slowly fluctuating part of the residual coupling usually using an Andersen−Weiss-type Ansatz for slow cooperative motions[54,55] frequently fail to support such a linearity,[23,25,56,57] and the cause is to be attributed to the nonapplicability of the underlying model.[16] Detailed proof based on temperature-dependent MQ experiments on NR will be published shortly under separate cover.

An intercept with the y-axis is commonly observed and must be attributed to local, lateral chain packing or entanglement constraints, to which the NMR phenomenon is more sensitive than equilibrium swelling:

$$\frac{1}{M_c(\text{NMR})} \approx \frac{1}{M_e} + \frac{1}{M_c(\text{swelling})} \quad (13)$$

This relation is, of course, simplified, as a certain fraction of the entanglements will not unfold ("desintersperse") upon swelling and form tight topological links which reduce the equilibrium swelling. The intercept should therefore be lower than expected, and the corresponding M_e should be higher than what is derived from, e.g., the plateau modulus of a high-molecular-weight melt.

The intercept for NR is low indeed, suggesting $M_e = 8.7$ kg/mol, which is higher than the rheological value of 6.2 kg/mol.[58,59] More importantly, the observed *slope* is about 2, showing that either NMR experiments *overestimate* molecular order or some assumptions in their interpretation are incorrect. Dividing the NMR data by 2 to achieve coincidence with the swelling results, a larger apparent $M_e = 17.4$ kg/mol is obtained. Apart from the overall factor of 2, the data are thus internally consistent, and the molar mass of chains between trapped entanglements in vulcanized NR is derived to be about $M_{te} = (1/6.2 - 1/17.4)^{-1} = 9.6$ kg/mol.

At this point, recall that the strand length distribution is exponential and that NMR yields a weight-averaged $1/M_c$ (each segment, not each chain, contributes to the signal). This should lead to *underestimated* order. As there is a factor of 2 between the weight and the number average (from swelling), one should expect M_c(NMR) to be a factor of 2 *lower* than the swelling result, in diametral contrast with the observation. Note, however, that the topological interactions discussed above effectively increase the order of long-chain contributions and thus bias this average and therefore screen the distribution effect to an unknown extent. In how far this specific bias is actually related to (trapped) entanglements in the traditional sense, and might partially explain the $1/M_e$ intercept, remains to be clarified.

Finally, consider the data for PDMS. Reassuringly, a plot of $1/M_c$ vs $1/M_{pre}$ (not shown) exhibits a linear relation with a slope of around 1 and an intercept from which the molecular weight between physical constraints is obtained as $M_{te} = 10.5 \pm 4$ kg/mol, which is close to $M_e \approx 12$ kg/mol. When the NMR data are plotted vs the $1/M_{pre}$ instead of $1/M_c$ (Figure 8), a left shift is observed, in agreement with the above discussion. Yet now, the slope for the NMR values is appreciably less than unity, indicating *underestimated* order. Note that the precursor polydispersities range between 1.5 and 2; thus, distribution effects on the NMR-detected order should be similar to the case of NR.

In further substantial contrast to the case of NR, the NMR-detected order due to local packing or entanglements ($\sim 1/M_e$) is grossly overestimated in PDMS, and multiplication of the NMR values by 2 to achieve unity slope even enhances this contrast. The NMR value for M_e would then be about 3 kg/mol. Thus, for PDMS, the NMR-determined and actual inter-cross-link and entanglement spacings cannot be reconciled with a simple scaling factor.

IV. Conclusions

In summary, it is seen that the NMR-detected chain order in networks bears no simple relation with the actual cross-link density, at least not within the established model framework explored herein. Though the overall scaling is found to be linear as expected (which can justify simple calibration procedures), the prefactor is not clear within a factor of the order of 2 in either direction. We have addressed some potential problems, e.g., the issue of distributions of end-to-end separations and chain lengths, which are nontrivially reflected in the NMR observable. More fundamental issues have been raised with respect to the accepted models treating the stiffness of real chains and its relationship with local-scale dynamics.[53] At this point, consider results from recent simulation work, which shows that NR and PDMS differ qualitatively in that the Rouse model is (expectedly) insufficient to take into account interchain effects on the conformational dynamics of the former, while it appears to hold for the latter.[60]

As to NMR-related problems, our previous computer simulations performed in collaboration with J.-U. Sommer indicated that the nontrivial way the NMR quantity is formed, i.e., as a running time average of a second-order tensor, might play a role.[45] This should be contrasted with, e.g., strain birefringence, in which the

polarizability tensor is simply ensemble-averaged in a snapshot-wise fashion.[26] The running average depends nontrivially on the fluctuation statistics, as is for instance evidenced by swelling in good solvent (excluded volume not screened), where counterintuitively the simulated NMR order parameter *decreases*. At any rate, statistically cross-linked vulcanized rubbers appear to behave qualitatively differently from end-linked PDMS networks, and our hope is that further computer simulations might help to clarify these issues.

In the first part of this paper, the quantitative relationship between the NMR-detected residual coupling and the actual order parameter has been reassessed, and in contrast to earlier work, it was found that the identification of backbone bonds with the symmetry axis of uniaxial segmental dynamics is not straightforward, as seemingly secondary couplings to protons in neighboring groups may become important upon rotational averaging. We believe that these limitations do not account for the major uncertainties addressed above, in particular because the data on NR and PDMS, where our spin dynamics modeling was performed on the basis of the same assumptions, deviate in different directions.

Some final comments should be added on the rather high NMR order parameters reported by Spiess and coworkers,[11] who have used DQ MAS NMR to derive $S_b \approx 0.2$ at $T = T_g + 50$ K at for un-cross-linked PB melts with roughly equal *cis* and *trans* contents. Even considering that *trans* units might exhibit twice the order of *cis* units, this observation clearly surpasses all our data for weakly cross-linked systems or melts. One might speculate that the used sample contains a high density of unexpected physical cross-links (e.g., crystallites). Importantly yet, the segmental averaging process is still ongoing at this temperature! In a forthcoming work, we will provide a consistent interpretation of T-dependent MQ data, which evidences that the length scale related to segmental averaging at $T = T_g + 50$ K is appreciably shorter than the spacing between entanglements or cross-links, such that higher temperatures are needed when lowly cross-linked samples are to be characterized.

In addition, the DQ MAS method used in the literature exhibits rather unfavorable relaxation properties, which are largely due to interference with the MAS time scale and accumulating experimental imperfections. Therefore, it was necessary to *calibrate* the DQ data using simple spinning sidebands, and it is possible that these are not of purely dipolar origin. A proof can be taken from the 2D DQ spectrum in Figure 1b, where the signals appear elongated along the diagonal, whereby a linear spin interaction (e.g., internal susceptibility contrast) is identified as an important source of line broadening. This stresses the advantages of the static MQ sequence used in this work, with its possibility to normalize for relaxation effects. This allows the direct measurement of residual couplings without calibration, at least in the case of samples with very high-molecular-weight[17] or permanent cross-links.

We conclude that despite its undisputed use in comparing samples and assessing relative differences in the cross-link density with good accuracy, the chain order phenomenon as seen by NMR is by far not fully understood, with uncertainties arising at various stages of theoretical modeling. It is our hope that this work can contribute a foundation with respect to the relation between the NMR-observed residual coupling and the order parameter associated with a single chain segment and initiate further work on an exact quantification.

Acknowledgment. Funding of this work was provided by the Deutsche Forschungsgemeinschaft (SFB 428), the Fonds der Chemischen Industrie, and the CICYT, MAT 2004-00825. M. A. López-Manchado thanks the Ministerio de Educación y Ciencia for the concession of a Ramon y Cajal contract. Robert Graf is acknowledged for valuable discussions.

References and Notes

(1) Litvinov, V. M., De, P. P., Eds.; *Spectroscopy of Rubbers and Rubbery Materials*; Rapra Technology Ltd.: Shawbury, 2002.
(2) Cohen-Addad, J. P.; Vogin, R. Molecular Motion Anisotropy as Reflected by a "Pseudosolid" Nuclear Spin−Echo: Observation of Chain Constraints in Molten *cis*-1,4-Polybutadiene. *Phys. Rev. Lett.* **1974**, *33*, 940−943.
(3) Cohen-Addad, J. P. NMR and Gel Elasticity Interrelationship. *Macromolecules* **1989**, *22*, 147−151.
(4) Cohen-Addad, J. P. NMR and Fractal Properties of Polymeric Liquids and Gels. *Prog. NMR Spectrosc.* **1993**, *25*, 1−316.
(5) Brereton, M. G. NMR Transverse Relaxation Function Calculated for Constrained Polymer Chains: Application to Entanglements and Networks. *Macromolecules* **1990**, *23*, 1119−1131.
(6) Saalwächter, K. Artifacts in Transverse Proton NMR Relaxation Studies of Elastomers. *Macromolecules* **2005**, *38*, 1508−1512.
(7) Saalwächter, K.; Herrero, B.; López-Manchado, M. A. Chemical Shift-Related Artifacts in NMR Determinations of Proton Residual Dipolar Couplings in Elastomers. *Macromolecules* **2005**, *38*, 4040−4042.
(8) Collignon, J.; Sillescu, H.; Spiess, H. W. Pseudo-solid echoes of proton and deuteron NMR in polyethylene melts. *Colloid Polym. Sci.* **1981**, *259*, 220−226.
(9) Callaghan, P. T.; Samulski, E. T. Molecular Ordering and the Direct Measurement of Weak Proton−Proton Dipolar Interactions in a Rubber Network. *Macromolecules* **1997**, *30*, 113−122.
(10) Demco, D. E. Hafner, S.; Fülber, C.; Graf, R.; Spiess, H. W. Two-dimensional proton magnetization-exchange NMR spectroscopy in cross-linked elastomers. *J. Chem. Phys.* **1996**, *105*, 11285−11296.
(11) Graf, R.; Heuer, A.; Spiess, H. W. Chain-Order Effects in Polymer Melts Probed by ^{1}H Double-Quantum NMR Spectrocopy. *Phys. Rev. Lett.* **1998**, *80*, 5738−5741.
(12) Graf, R.; Demco, D. E.; Hafner, S.; Spiess, H. W. Selective residual dipolar couplings in cross-linked elastomers by ^{1}H double-quantum NMR spectroscopy. *Solid State Nucl. Magn. Reson.* **1998**, *12*, 139−152.
(13) Schneider, M.; Gasper, L.; Demco, D. E.; Blümich, B. Residual dipolar couplings by ^{1}H dipolar-encoded longitudinal magnetization, double- and triple-quantum nuclear magnetic resonance in cross-linked elastomers. *J. Chem. Phys.* **1999**, *111*, 402−415.
(14) Saalwächter, K.; Ziegler, P.; Spyckerelle, O.; Haidar, B.; Vidal, A.; Sommer, J.-U. ^{1}H multiple-quantum nuclear magnetic resonance investigations of molecular order distributions in poly(dimethylsiloxane) networks: Evidence for a linear mixing law in bimodal systems. *J. Chem. Phys.* **2003**, *119*, 3468−3482.
(15) Saalwächter, K. Detection of Heterogeneities in Dry and Swollen Polymer Networks by Proton Low-Field NMR Spectroscopy. *J. Am. Chem. Soc.* **2003**, *125*, 14684−14685.
(16) Saalwächter, K. ^{1}H multiple-quantum nuclear magnetic resonance investigations of molecular order in polymer networks: Intensity decay, I.; restricted slow dynamics. *J. Chem. Phys.* **2004**, *120*, 454−664.
(17) Saalwächter, K.; Klüppel, M.; Luo, H.; Schneider, H. Chain Order in Filled SBR Elastomers: A Proton Multiple-Quantum NMR Study. *Appl. Magn. Reson.* **2004**, *27*, 4071−417.
(18) Gotlib, Yu. Ya.; Lifshitz, M. I.; Shevelev, V. A.; Lishanskij, I. S.; Balanina, I. V. *Vysokomol. Soedin. A18* **1976**, *10*, 2299.
(19) Fry, Ch. G.; Lind, A. C. Determination of Cross-Link Density in Thermoset Polymers by Use of Solid-State ^{1}H NMR Techniques. *Macromolecules* **1988**, *21*, 1292−1297.

(20) Simon, G.; Birnstiel, A.; Schimmel, K.-H. Network characterisation of end-linked poly(dimethylsiloxane) by ^{1}H NMR spin−spin relaxation. *Polym. Bull. (Berlin)* **1989**, *21*, 235−241.
(21) Sotta, P.; Fülber, C.; Demco, D. E.; Blümich, B.; Spiess, H. W. Effect of Residual Dipolar Interactions on the NMR Relaxation in Cross-Linked Elastomers. *Macromolecules* **1996**, *29*, 6222−6230.
(22) Cohen-Addad, J. P.; Thanh, B. P.; Montes, H. Evidence for a Linear NMR-Elasticity Interrelationship in Polymeric Gels. *Macromolecules* **1997**, *30*, 4374−4380.
(23) Fischer, E.; Grinberg, F.; Kimmich, R.; Hafner, S. Characterization of polymer networks using the dipolar correlation effect on the stimulated echo and field-cycling nuclear-magnetic resonance relaxometry. *J. Chem. Phys.* **1998**, *109*, 846−854.
(24) Knörgen, M.; Menge, H.; Hempel, G.; Schneider, H.; Ries, M. E. Relationship between the transverse NMR decay and the dipolar interaction in elastomers: a comparison of two models. *Polymer* **2002**, *43*, 4091−4096.
(25) Maxwell, R. S.; Balazs, B. Residual dipolar coupling for the assessment of cross-link density changes in γ-irradiated silica-PDMS composite materials. *J. Chem. Phys.* **2002**, *116*, 10492−10502.
(26) Kuhn, W.; Grün, F. Beziehungen zwischen elastischen Konstanten und Dehnungsdoppelbrechung hochelastischer Stoffe. *Kolloid-Z.* **1942**, *101*, 248−271.
(27) Flory, P. J. *Principles of Polymer Chemistry*; Cornell University Press: Ithaca, NY, 1953.
(28) Ries, M. E.; Brereton, M. G.; Ward, I. M.; Cail, J. I.; Stepto, R. F. T. Rescaling Approach to Molecular Orientation for NMR and Optical Properties of Polymer Networks. *Macromolecules* **2002**, *35*, 5665−5669.
(29) López-Manchado, M. A.; Herrero, B.; Arroyo, M. Preparation and characterization of organoclay nanocomposites based on natural rubber. *Polym. Int.* **2003**, *52*, 1070−1077.
(30) López-Manchado, M. A.; Arroyo, M.; Herrero, B.; Biagiotti, J. Vulcanization kinetics of natural rubber-organoclay nanocomposites. *J. Appl. Polym. Sci.* **2003**, *89*, 1−15.
(31) Varghese, S.; Karger-Kocsis, J.; Gatos, K. G. Melt compounded epoxidized natural rubber/layered silicate nanocomposites: structure-properties relationships. *Polymer* **2003**, *44*, 3977−3983.
(32) Flory, P. J. Statistical Mechanics of Swelling of Network Structures. *J. Chem. Phys.* **1950**, *18*, 108−111.
(33) Baum, J.; Pines, A. Multiple-Quantum NMR Studies of Clustering in Solids. *J. Am. Chem. Soc.* **1986**, *108*, 7447−7454.
(34) Bak, M.; Rasmussen, J. T.; Nielsen, N. C. SIMPSON: A General Simulation Program for Solid-State NMR Spectroscopy. *J. Magn. Reson.* **2000**, *147*, 296−330.
(35) Graf, R. Hochauflösende Doppelquanten-NMR−Spektroskopie an amorphen Polymeren, Dissertation, Universität Mainz, Shaker Verlag, Aachen, 1998.
(36) Natta, G.; Corradini, P. The Crystal Structure of *cis*-1,4-Polybutadiene. *Nuovo Cim. Suppl.* **1960**, *25*, 111−121.
(37) Nyburg, S. C. A Statistical Structure for Crystalline Rubber. *Acta Crystallogr.* **1954**, *7*, 385−392.
(38) Immirzi, A. Tedesco, C.; Monaco, G.; Tonelli, A. E. Crystal Structure and Melting Entropy of Natural Rubber. *Macromolecules* **2005**, *38*, 1223−1231.
(39) Mark, J. E. Random-Coil Configurations of *cis*-1,4-Polybutadiene and *cis*-1,4-Polyisoprene. Theoretical Interpretation. *J. Am. Chem. Soc.* **1966**, *88*, 4354−4359.
(40) Sen, T. Z.; Bahar, I.; Erman, B.; Lauprêtre, F.; Monnerie, L. Local Dynamics of *cis*-1,4-Polybutadiene and *cis*-1,4-Polyisoprene. A Comparative Study Based on Cooperative Kinematics Theory and NMR Experiments. *Macromolecules* **1999**, *32*, 3017−3024.
(41) Doxastakis, M.; Mavrantzas, V. G.; Theodorou, D. N. Atomistic Monte Carlo simulation of *cis*-1, 4 polyisoprene melts. I. Single temperature end-bridging Monte Carlo simulations. *J. Chem. Phys.* **2001**, *115*, 11339−11351.
(42) Wang, M.; Bertmer, M.; Demco, D. E.; Blümich, B. Segmental and Local Chain Mobilities in Elastomers by ^{13}C-^{1}H Residual Heteronuclear Dipolar Couplings. *J. Phys. Chem. B* **2004**, *108*, 10911−10918.
(43) Saalwächter, K.; Kleinschmidt, F.; Sommer, J.-U. Swelling Heterogeneities in End-Linked Model Networks: A Combined Proton Multiple-Quantum NMR and Computer Simulation Study. *Macromolecules* **2004**, *37*, 8556−8568.
(44) Schuld, N.; Wolf, B. A. Solvent Quality as Reflected in Concentration- and Temperature-Dependent Flory-Huggins Interaction Parameters. *J. Polym. Sci., Part B: Polym. Phys.* **2001**, *39*, 651−662.
(45) Sommer, J.-U.; Saalwächter, K.. Segmental Order in Endlinked Polymer Networks: A Monte Carlo Study. *Eur. Phys. J. E,* submitted for publication.
(46) Stockmayer, W. H. Theory of Molecular Size Distribution and Gel Formation in Branched Polymers II. General Cross Linking. *J. Chem. Phys.* **1944**, *12*, 125−131.
(47) Sotta, P.; Deloche, B. Uniaxiality Induced in a Strained Poly(dimethylsiloxane) Network. *Macromolecules* **1990**, *23*, 1999−2007.
(48) Brereton, M. G. NMR Study of the Molecular Anisotropy Induced in a Strained Rubber Network. *Macromolecules* **1993**, *26*, 1152−1157.
(49) Warner, M. Callaghan, P. T.; Samulski, E. T. Nuclear Magnetic Resonance Line Shape from Strained Gaussian Networks. *Macromolecules* **1997**, *30*, 4733−4736.
(50) Kornfield, J. A.; Chung, G.-C.; Smith, S. D. Reconsideration of Deuterium NMR Observations of Orientational Coupling in Polymer Networks in Light of Motional Hetergeneity in Styrene-d_8−Styrene Block Copolymers. *Macromolecules* **1992**, *25*, 4442−4444.
(51) Flory, P. J. *Statistical Mechanics of Chain Molecules*; Hanser: München, 1975.
(52) Smith, G. D.; Paul, W. United Atom Force Field for Molecular Dynamics Simulations of 1,4-Polybutadiene Based on Quantum Chemistry Calculations on Model Molecules. *J. Phys. Chem. A* **1998**, *102*, 1200−1208.
(53) Ding, Y. Kisliuk, A.; Sokolov, A. P. When Does a Molecules Become a Polymer? *Macromolecules* **2004**, *37*, 161−166.
(54) Ball, R. C.; Callaghan, P. T.; Samulski, E. T. A simplified approach to the interpretation of nuclear spin correlations in entangled polymeric liquids. *J. Chem. Phys.* **1997**, *106*, 7352−7361.
(55) Kimmich, R. *NMR Tomography, Diffusometry, Relaxometry*; Springer: Berlin, 1997.
(56) Grinberg, F.; Garbarczyk, M.; Kuhn, W. Influence of the cross-link density and the filler content on segment dynamics in dry and swollen natural rubber studied by the NMR dipolar-correlation effect. *J. Chem. Phys.* **1999**, *111*, 11222−11231.
(57) Fechete, R.; Demco, D. E.; Blümich, B. Chain orientation and slow dynamics in elastomers by mixed magic-Hahn echo decays. *J. Chem. Phys.* **2003**, *118*, 2411−2421.
(58) Graessley, W. W. The Entanglement Concept in Polymer Physics. *Adv. Polym. Sci.* **1974**, *16*, 1−177.
(59) Abdel-Goad, M.; Pyckhout-Hintzen, W.; Kahle, S.; Allgaier, J.; Richter, D.; Fetters, L. J. Rheological Properties of 1,4-Polyisoprene over a Large Molecular Weight Range. *Macromolecules* **2004**, *37*, 8135−8144.
(60) Krushev, S.; Paul, W.; Smith, G. D. The Role of Internal Rotational Barriers in Polymer Melt Chain Dynamics. *Macromolecules* **2002**, *35*, 4198−4203.

MA051238G